

Electronic Supplementary Information

Nanoporous Gyroid Ni/NiO/C Nanocomposite from Block Copolymer Template with High Capacity and Stability for Lithium Storage

Chung-Fu Cheng¹, Yu-Ming Chen¹, Feng Zou¹, Kai-Chieh Yang², Tzu-Ying Lin³, Kewei Liu¹, Chi-Huang Lai³, Rong-Ming Ho^{2*} and Yu Zhu^{1*}

¹ Department of Polymer Science, the University of Akron, 170 University Circle, Ohio 44325, USA.

² Department of Chemical Engineering, National Tsing Hua University, Hsinchu 30010, Taiwan

³ Department of Materials Science and Engineering, National Tsing Hua University, Hsinchu 30010, Taiwan

(a,b) SEM micrographs of PS/Ni nanohybrids. (c) XRD for PS/Ni nanohybrids

Temperature profile for the modified calcination process. The red dash line shows the separation of the temperature region into 1st stage (Template removal) and 2nd stage (Ni oxidation), respectively.

One-dimensional XRD profile of the 3D NiO/Ni nanocomposite after the first stage calcination and air quench to the room temperature.

XPS spectrum of nanoporous gyroid Ni/NiO nanocomposite.

FESEM micrograph of the nanoporous gyroid Ni/NiO/C nanocomposite in small magnification mode.

(a) BET results and (b) pore-size distribution of nanoporous gyroid Ni/NiO/C nanocomposite.

XPS spectrum of nanoporous gyroid Ni/NiO/C nanocomposite.

(a) Ni 2p XPS spectrum, (b) O 1s XPS spectrum, (c) C 1s XPS spectrum.

Thermogravimetric Analysis (TGA) results for the nanoporous gyroid Ni/NiO/C nanocomposite under air purge.

Ratability comparison between our work and previous reports. The nanoporous gyroid Ni/NiO/C nanocomposite in this work exhibited better ratability than previous reports of NiO based electrode.

(a) SEM micrograph of Ni/NiO/C composite prepared as sheet film. (b) Corresponding XRD profile (c) Specific capacity of nanoporous gyroid Ni/NiO/C nanocomposite anode as a function of cycling number at the current density of 1 A/g. The sheet-film Ni/NiO/C anode was subject to a sudden capacity loss at the 187th cycle. (d) Comparison of specific capacity of nanoporous gyroid Ni/NiO/C nanocomposite (black) and Ni/NiO/C sheet film composite (red).

Charge/Discharge profiles at different cycle number. (current density = 1 A/g)

Nyquist plots of the nanoporous gyroid Ni/NiO/C nanocomposite electrode after different cycles. The spectra were measured over the frequency range from 1 MHz to 0.01 Hz. Inset shows the equivalent circuit used for data fitting.

TEM image of nanoporous gyroid Ni/NiO/C nanocomposite electrode after 1000 cycles.

Table S1. Comparison of the element parameters from the equivalent circuit in Figure S12.

Table S2. Comparison of cycle performance for NiO based LIBs.

Microscopy (TEM)

TEM observations were performed on a JEOL-6210 or JEOL, JEM-ARM200 FTH using accelerating voltages of 200 keV. Before observations, the bulk samples were prepared by microtome to slice thin sections with the thickness of 50 nm for TEM observation.

Microscopy (FESEM)

FESEM observations were performed on a JEOL JSM-6700F or FEI Quanta450 using accelerating voltages of 3-10 keV. Before observations, the samples were sputter-coated with 2-3 nm of platinum to avoid the charge effect (the platinum coating thickness was estimated from a calculated deposition rate and experimental deposition time).

Small-angle X-ray Scattering (SAXS)

Small-angle X-ray scattering (SAXS) experiments were conducted at the synchrotron X-ray beam-line X27C at the National Synchrotron Radiation Research Center (NSRRC) in Hsinchu. The wavelength of the X-ray beam was 0.155 nm. A MAR CCD X-ray detector (MAR USA) was used to collect the two-dimensional (2D) SAXS patterns. One-dimensional (1D) linear profile was obtained by integration of the 2D pattern. The scattering angle of the SAXS pattern was calibrated using silver behenate, with the first-order scattering vector q ($q = 4\lambda^{-1} \sin\theta$, where 2θ is the scattering angle) being 1.076 nm^{-1} .

X-ray Diffraction (XRD)

To further confirm the structure of the ordered nanoporous gyroid Ni/NiO/C and Ni/NiO nanocomposites, powder sample was prepared and performed a XRD experiment. The crystal

structure of the as-prepared product was characterized by XRD using a Rigaku Ultima IV X-ray diffractometer with Cu KR radiation ($\lambda = 0.1542$ nm). The scanning 2θ angle ranged between 20° and 70° with a step scanning of 1° for 1 s.

Thermogravimetric Analysis (TGA)

TGA analyses were carried out using Q500 (TA Instruments) under air purge. The temperature was increased with a temperature ramp rate of $5^\circ\text{C}/\text{min}$ up to 750°C to complete the characterization of C, Ni and NiO weight percentage. The Carbon content was calculated directly by the weight loss from $300\text{--}550^\circ\text{C}$ resulting from the carbon decomposition and the Ni content was calculated by the weight gain due to the oxidation of remained Ni from 550°C - 750°C .

X-ray Photon Spectroscopy (XPS)

XPS analysis was performed by ULVAC-PHI XPS under Scanning Monochromated Al anode. Bulk sample was prepared and the corresponding spectra were demonstrated in Fig S5 and S6. The XPS data was measured and collected under 180° spherical capacitor analyzer with 32 channel detector.

Preparation of Ni/NiO/C Composite as Sheet Film

A fresh growth aqueous solution consisting of NiCl_2 (0.4 g), hydrazinium hydroxide (4 ml), ammonium hydroxide (6.4 ml), DI water (40 ml) and methanol (40 ml) was prepared under temperature about 60°C to grow the Ni. After one day of the reaction, the Ni ion was reduced into Ni and form a condensed sheet film from the solution. Ni sheet film was collected and performed under same annealing process (i.e. same temperature profile in Fig S2) to oxidize the Ni into NiO.

After the Ni/NiO composite was formed, same carbon coating process was performed to fabricate Ni/NiO/C composite.

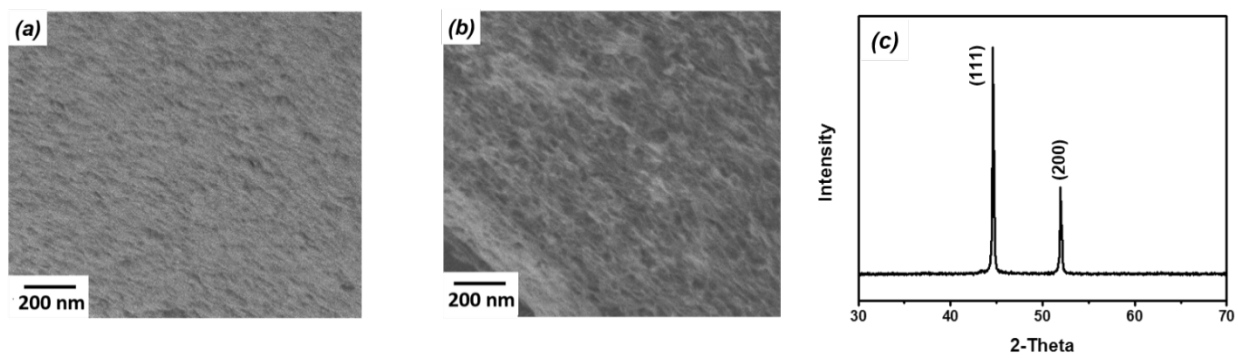


Figure S1. (a,b) SEM micrographs of PS/Ni nanohybrids. (c) XRD profile for PS/Ni nanohybrids

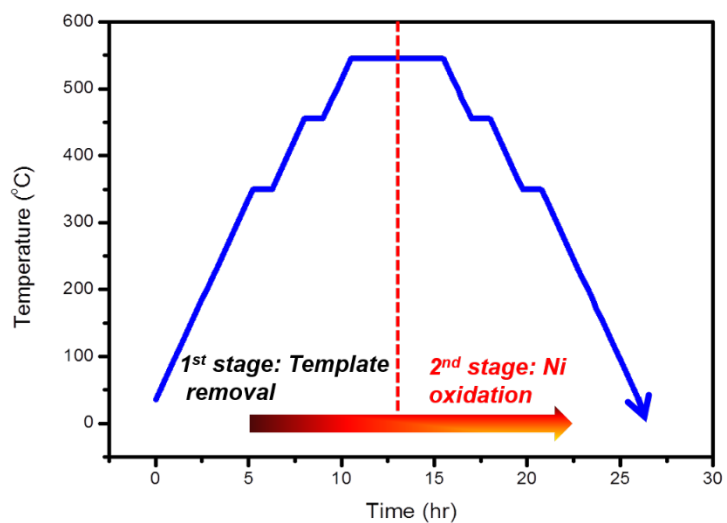


Figure S2. Temperature profile for the modified calcination process. The red dash line shows the separation of the temperature region into 1st stage (Template removal) and 2nd stage (Ni oxidation), respectively.

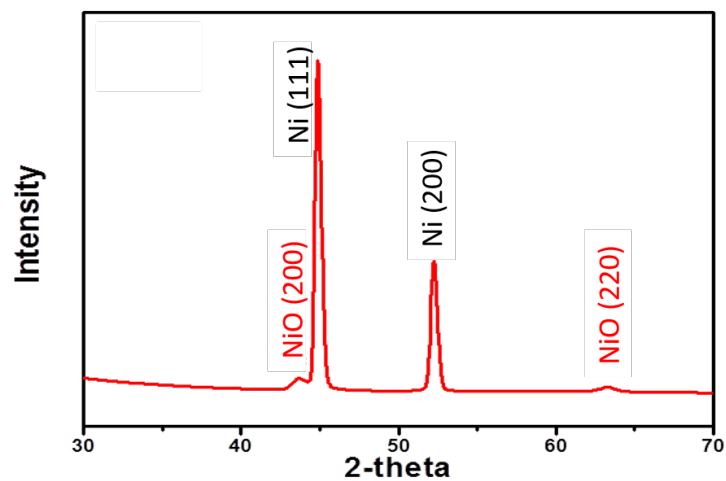


Figure S3. One-dimensional XRD profile of the 3D NiO/Ni nanocomposite after the first stage calcination and air quench to the room temperature.

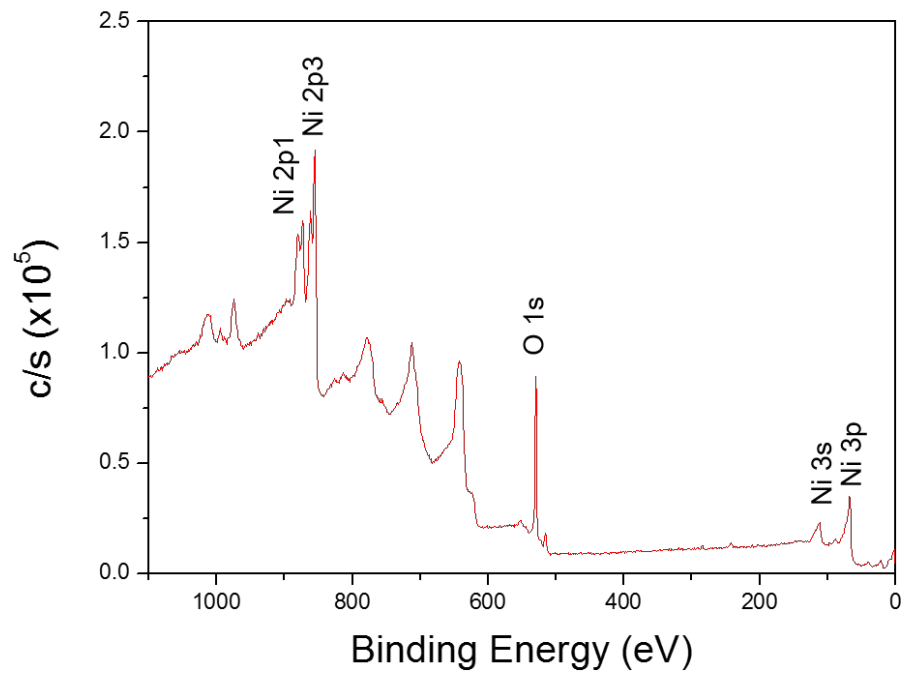


Figure S4. XPS spectrum of nanoporous gyroid Ni/NiO nanocomposite.



Figure S5. FESEM micrograph of the nanoporous gyroid Ni/NiO/C nanocomposite in small magnification mode.

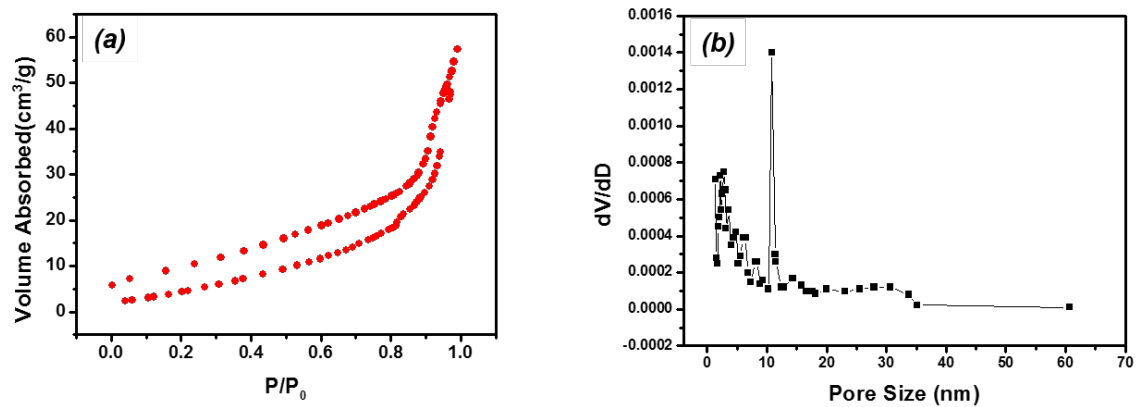


Figure S6. (a) BET results and (b) pore-size distribution of nanoporous gyroid Ni/NiO/C nanocomposite.

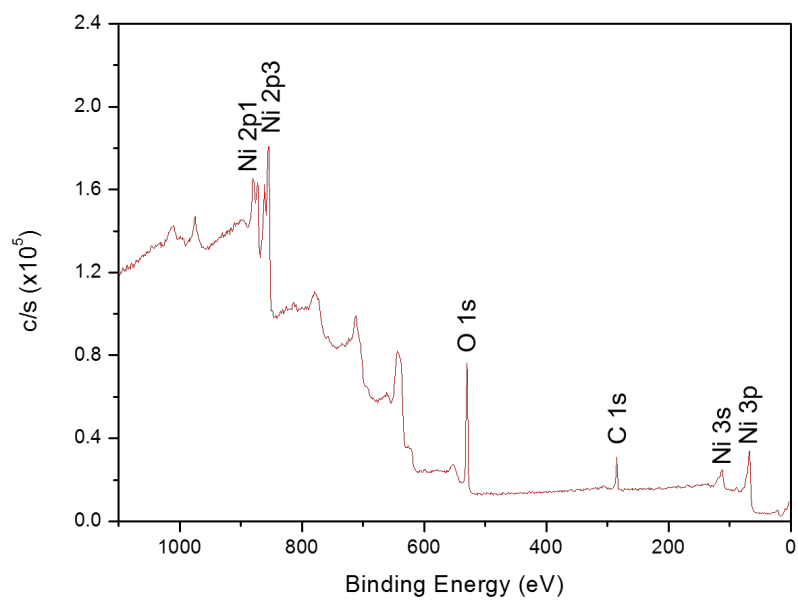


Figure S7. XPS spectrum of nanoporous gyroid Ni/NiO/C nanocomposite.

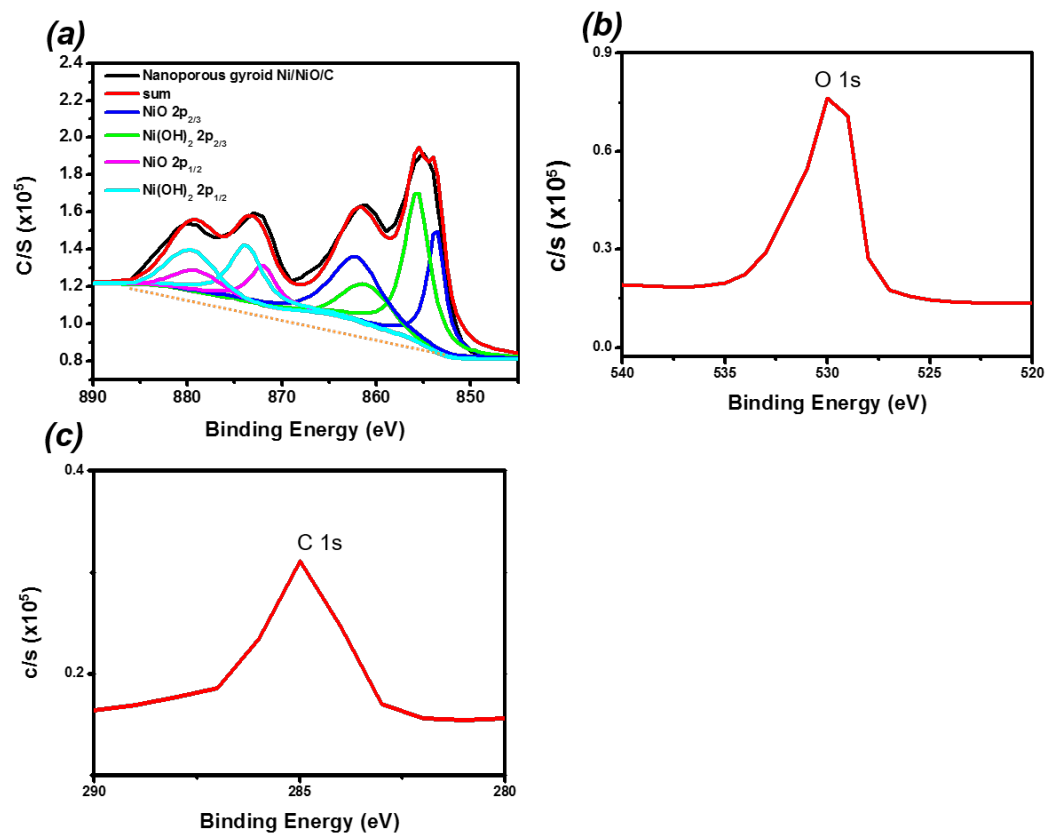


Figure S8. (a) Ni 2p XPS spectrum, (b) O 1s XPS spectrum, (c) C 1s XPS spectrum.

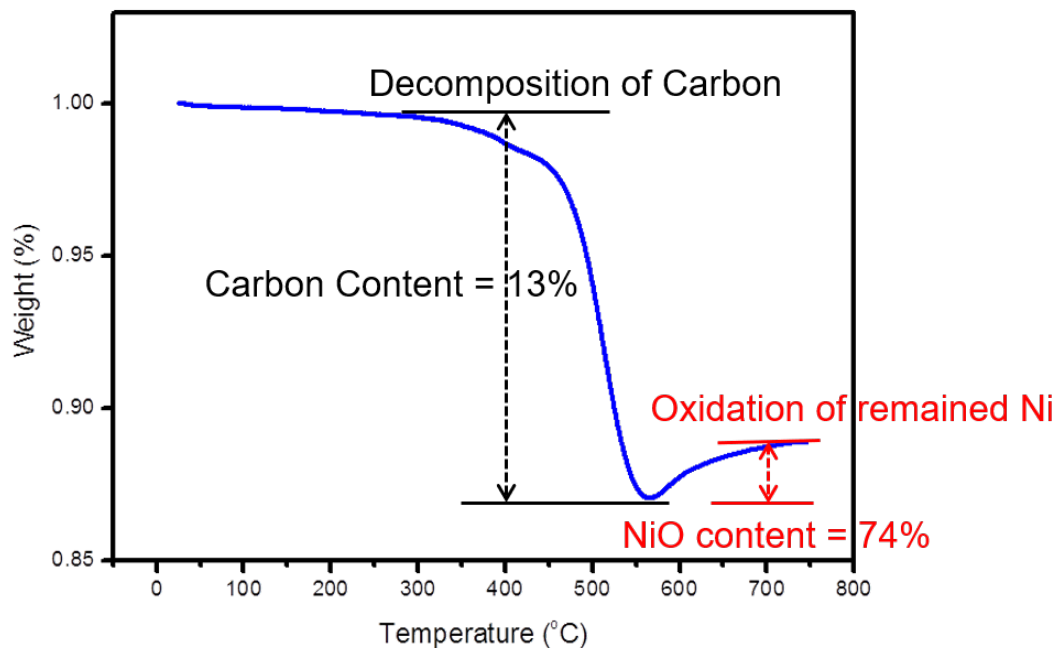


Figure S9. Thermogravimetric Analysis (TGA) results for the nanoporous gyroid Ni/NiO/C nanocomposite under air purge.

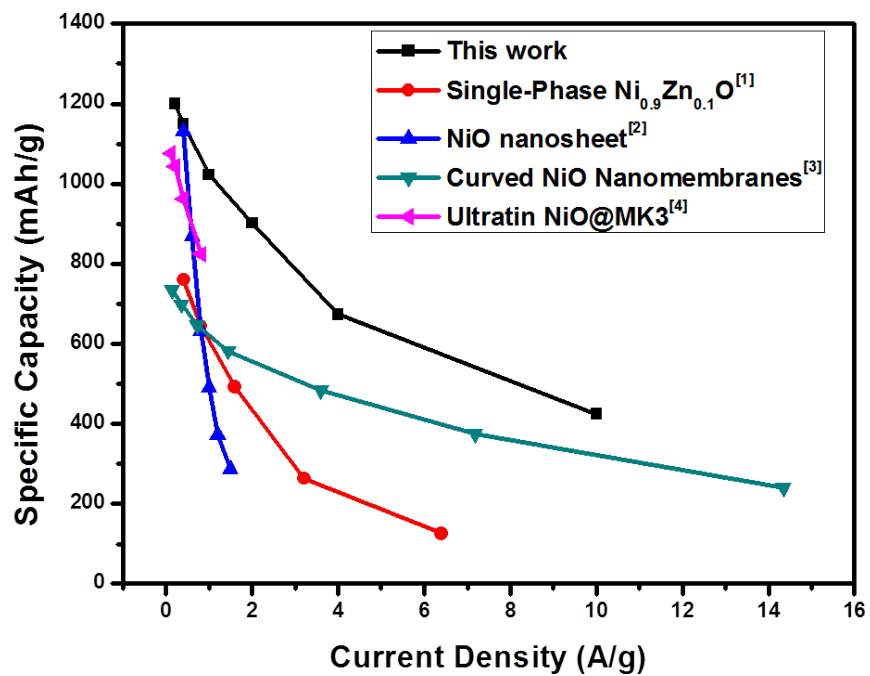


Figure S10. Ratability comparison between our work and previous reports. The nanoporous gyroid Ni/NiO/C nanocomposite in this work exhibited better ratability than previous reports of NiO based electrode.

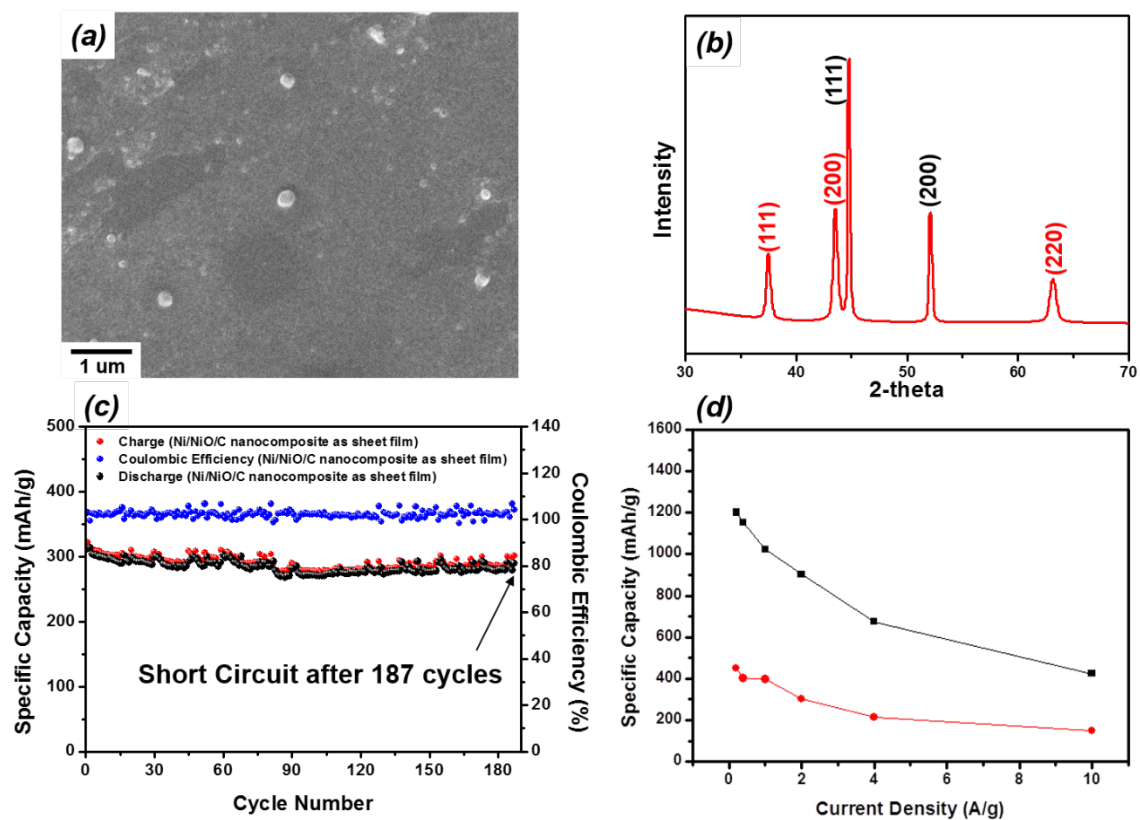


Figure S11. (a) SEM micrograph of Ni/NiO/C composite prepared as sheet film. (b) XRD profile of Ni/NiO/C sheet film composite (c) Specific capacity of nanoporous gyroid Ni/NiO/C nanocomposite anode as a function of cycling number at the current density of 1 A/g. The sheet-film Ni/NiO/C anode was subject to a sudden capacity loss at the 187th cycle. (d) Comparison of specific capacity of nanoporous gyroid Ni/NiO/C nanocomposite (black) and Ni/NiO/C sheet film composite (red).

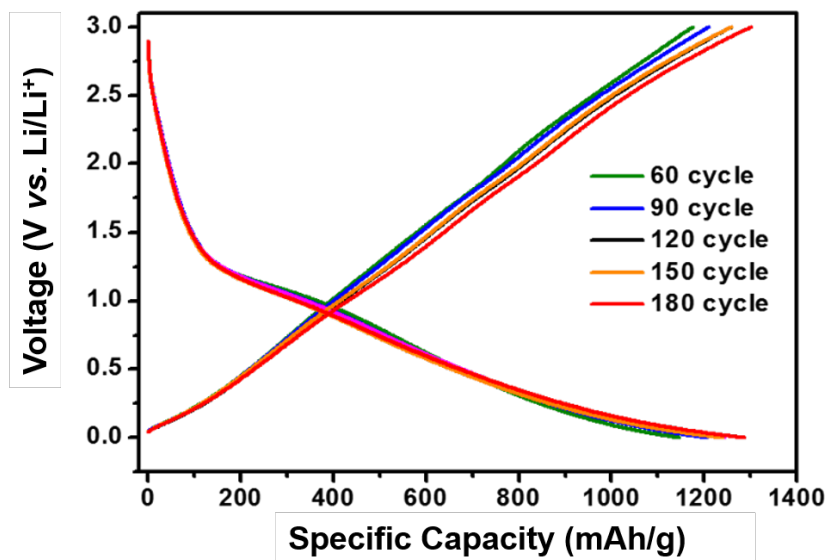


Figure S12. Charge/Discharge profiles of nanoporous gyroid Ni/NiO/C nanocomposite at different cycle numbers. (current density = 1 A/g)

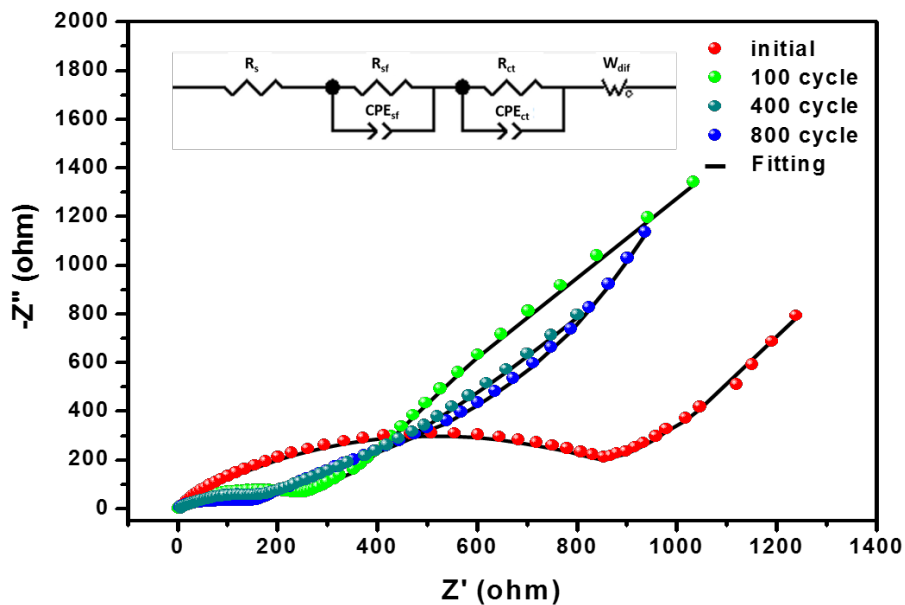


Figure S13. Nyquist plots of the nanoporous gyroid Ni/NiO/C nanocomposite electrode after different cycles. The spectra were measured over the frequency range from 1 MHz to 0.01 Hz. Inset shows the equivalent circuit used for data fitting.

Table S1. Comparison of the element parameters from the equivalent circuit in Figure S12.

Cycle	R_s (ohm)	R_{sf} (ohm)	CPE_{sf} (F)	R_{ct} (ohm)	CPE_{ct} (F)	Warburg Constant
Initial	2.79	58.7	0.92	732.6	0.79	747.9
100 Cycle	2.23	33.5	0.86	112.6	0.68	844.6
400 Cycle	2.66	45.3	0.91	91.3	0.70	710.5
800 Cycle	2.61	37.4	0.84	87.3	0.66	781.2

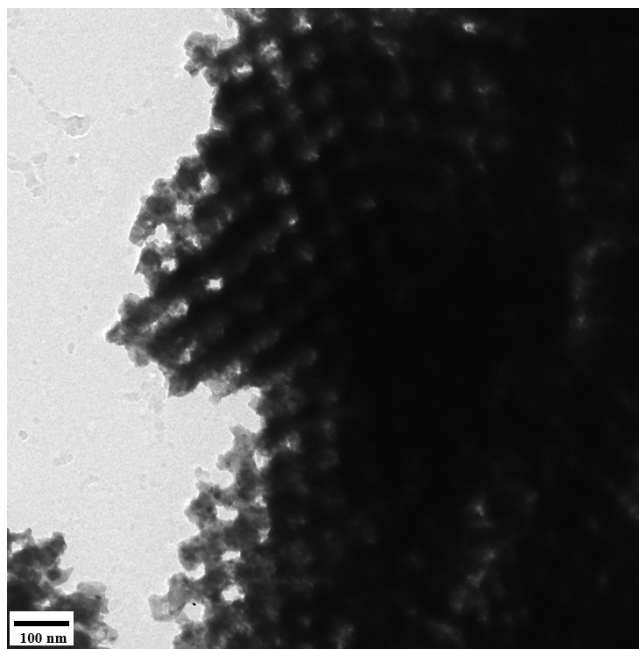


Figure S14. TEM image of nanoporous gyroid Ni/NiO/C nanocomposite electrode after 1000 cycles.

Table S2. Comparison of cycle performance for NiO based LIBs.

	Current Density	Specific Capacity	Cycle Number	Retention
Single-Phase Ni _{0.9} Zn _{0.1} O ^[1]	400 mA/g	760 mAh/g	200	~75%
NiO nanosheets ^[2]	200 mA/g	1300 mAh/g	130	~55%
Curved NiO Nanomembranes ^[3]	1077 mA/g	~800 mAh/g	1400	~90%
Ultrathin NiO nanosheets ^[4]	400 mA/g	848 mAh/g	50	90.2%
Ni/NiO hybrid nanomembranes ^[5]	1800 mA/g	743 mAh/g	900	Not mentioned
Ni–NiO nanofiber ^[6]	2150 mA/g	900 mAh/g	>1000	Not mentioned
NiO/Ni/Graphene ^[7]	2000 mA/g	942 mAh/g	1000	Not mentioned
This work (Nanoporous gyroid Ni/NiO/C nanocomposite)	1000 mA/g	1151 mAh/g	1000	70.2%

References

- [1] Huang, G.; Guo, X.; Cao, X.; Tian Q.; Sun, H. 3D Network Single-Phase Ni_{0.9}Zn_{0.1}O as Anode Materials for Lithium-Ion Batteries. *Nano Energy* **2016**, *28*, 338-345.
- [2] Zhu, Y.; Guo, H.; Wu, Y.; Cao, C.; Tao S.; Wu, Z. Surface-enabled superior lithium storage of high-quality ultrathin NiO nanosheets. *J. Mater. Chem. A* **2014**, *2*, 7904–7911.
- [3] Sun, X.; Yan, C.; Chen, Y.; Si, W.; Deng, J.; Oswald, S.; Liu, L.; Schmidt, O. G. Three-Dimensionally “Curved” NiO Nanomembranes as Ultrahigh Rate Capability Anodes for Li-Ion Batteries with Long Cycle Lifetimes. *Adv. Energy Mater.* **2014**, *4*, 1300912.
- [4] Fan, Z.; Liang, J.; Yu, W.; Ding, S.; Cheng, S.; Yang, G.; Wang, Y.; Xi, Y.; Xi, K.; Kumar, R. V. Ultrathin NiO Nanosheets Anchored on a Highly Ordered Nanostructured Carbon as an Enhanced Anode Material for Lithium Ion Batteries. *Nano Energy* **2015**, *16*, 152-162.
- [5] Sun, X.; Si, W.; Liu, X.; Deng, J.; Xi, L.; Liu, L.; Yan, C.; Schmidt, O. G. Multifunctional Ni/NiO Hybrid Nanomembranes as Anode Materials for High-Rate Li-Ion Batteries. *Nano Energy* **2014**, *9*, 168-175.
- [6] Bella, J.; Yeb, R.; Ahmedc, K.; Liu, C.; Ozkanc, M.; Ozkana, C. S. Free-Standing Ni–NiO Nanofiber Cloth Anode for High Capacity and High Rate Li-Ion Batteries. *Nano Energy* **2015**, *18*, 47-56.
- [7] Zou, F.; Chen, Y. M.; Liu, K.; Yu, Z.; Liang, W.; Bhaway, S. M.; Gao, M.; Zhu, Y. Metal Organic Frameworks Derived Hierarchical Hollow NiO/Ni/Graphene Composites for Lithium and Sodium Storage. *ACS Nano* **2016**, *10*, 377-386..